Invited Articles

Spreading on textiles: Dynamics of drops on model poroelastic fibrous materials

P. Van de Velde,[1] H. Madkour,[1] S. Protière,[2] and C. Duprat[1]

[1]*LadHyX, Département de Mécanique, CNRS - École Polytechnique, Institut Polytechnique de Paris, UMR 7646, F-91128 Palaiseau Cedex, France*

[2]*Institut Jean le Rond d'Alembert, Sorbonne Université, CNRS UMR 7190, F-75005 Paris, France*

(Received 6 June 2024; accepted 28 October 2024; published 17 April 2025)

When wetting drops are deposited on textiles, such as paper or cotton fabrics, their spreading is generally accompanied with absorption of the liquid into the fibrous material and often expansion (i.e., swelling), which may cause large deformations. Using experimental model systems, we consider the coupled effects of perfect wetting, capillary forces, and liquid absorption and swelling. On a flat poroelastic substrate, a wetting drop readily spreads; spreading is only limited by the absorption within the material, leading to a maximal wetted radius and a localized deformation that slows down the absorption. On an assembly of fibers, a wetting drop adopts a compact shape that is governed by the fiber's geometry. On a single fiber, this finite spreading leads to a large absorption time as the fiber becomes quickly saturated below the drop, leaving only slow diffusion towards the unsaturated regions to absorb the liquid. This time may be strongly reduced if the drop is allowed to spread, which is possible between two parallel fibers, provided the distance between them is small enough. As a drop applies a capillary force on the fibers, it may deform them, reducing the distance between them and inducing a spontaneous spreading. For favorable solvents that can penetrate and swell the fibers, swelling can further induce a spontaneous collapse of adjacent fibers, and thus a rapid absorption. On a fibrous grid, where spreading decreases with increasing porosity, localized swelling induces a large out-of-plane deformation of the mesh, forming a bulge whose shape depends on the grid pattern. All these effects affect the spreading dynamics and absorption times of drops on fibrous assemblies, and we rationalize these observations with models coupling wetting, poroelasticity, and elastocapillarity.

DOI: 10.1103/PhysRevFluids.10.040501

I. INTRODUCTION

When a drop is deposited on a porous material, it both spreads at its surface and imbibes into the porous structure. For example, a drop placed on a textile (e.g., a woven fabric or a nonwoven sheet of paper) will form an intricate stain, as the spreading of the liquid on the textile is accompanied by imbibition in pores of different sizes. Indeed, liquid may flow in the space between yarns or fibers, as well as in the finer intrayarn pores, as films along filaments, or inside the fibers themselves [1]. The complexity of such systems may be illustrated by a simple experiment, for example, by placing a drop of water on a sheet of paper (Fig. 1). As the drop spreads on the surface, it also imbibes within the fibrous structure [Fig. 1(a)] and inside the cellulosic fibers that absorb water and swell. The swelling of the fibers leads to large-scale deformations that are quickly visible (i.e., the sheet forms a bulge). When wetting a larger portion of paper (for example, by dragging a wet finger on the sheet), we can quickly see the development of regularly spaced wrinkles, whose shape depends on the direction of the wet strip [2] [Fig. 1(b)]. Indeed, paper sheets are usually anisotropic, as most fibers are aligned in the machine direction during the manufacturing processes. Here, the

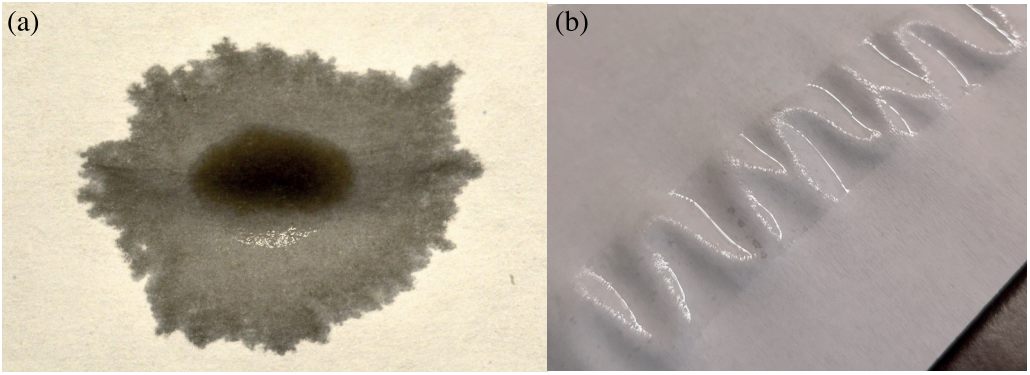

FIG. 1. Spreading on paper: (a) drop of dyed water as it spreads and imbibes into a sheet of copy paper, and (b) swelling and wrinkling of wet copy paper.

wrinkles are a direct observation of this underlying microstructure [2,3]. If you wet a strip in the other direction, you will see one or two parallel wrinkles instead of the pattern shown here; whatever direction you choose to wet, the wrinkles will be aligned along the main fiber direction. To check the main fiber direction in your piece of paper, look at the way the sheet bends under its own weight (it will sag more in the transverse direction, as the bending rigidity is lower than along the fiber's direction) or tear it and look at the crack path, which tends to follow the main fiber's direction; more quantitative measurements of paper anisotropy and fiber orientations are done with various methods, for example, by measuring macroscopic mechanical properties such as tensile strength or elastic modulus, or by visualizing the microstructure with x-ray microtomography or optical methods [4–6].

In these systems there is a combination of spreading, due to surface tension, imbibition into the porous underlying structure, and swelling of the material. Our approach has been to build model systems of increasing complexity in order to isolate the mechanisms at play in these complex situations. We consider minimal fibrous systems, from one fiber to thin woven fibrous meshes, and discuss the peculiar case of two parallel fibers. We only consider perfect wetting conditions, i.e., liquid and/or fiber systems where the equilibrium contact angle is nearly zero ($\theta_e \simeq 0^\circ$). In order to investigate the effect of swelling, we focus on elastomeric materials (typically silicone elastomer) that are perfectly wetted and swollen by silicone oils. Here, we will discuss the combined spreading and swelling of a drop on a flat substrate, on a single fiber, between two fibers, and finally, on a simple mesh. These model experiments serve as the first step to gain insight into the complex wetting of textiles. These mechanisms are present in a large variety of situations involving the interaction of a fibrous structure and liquids, e.g., stains on fabrics, inkjet printing on paper, aerosol filtration, or fog collection with fibrous nets.

II. DROPS ON FIBERS AND FIBROUS MATERIALS

In total wetting situations, where $\theta_e = 0$, a drop on a flat substrate spreads until its height becomes comparable to the size of a single fluid molecule and may thus reach large final radii. On a curved substrate, such as a fiber, the liquid spreads to join the fiber with a zero contact angle but has to match the curvature of the surface at the contact line. This limits its spreading to a finite length ℓ, as its static equilibrium shape is given by a balance between the Laplace pressure and the hydrostatic pressure:

$$\Delta p = \gamma\kappa = c - \rho g z, \tag{1}$$

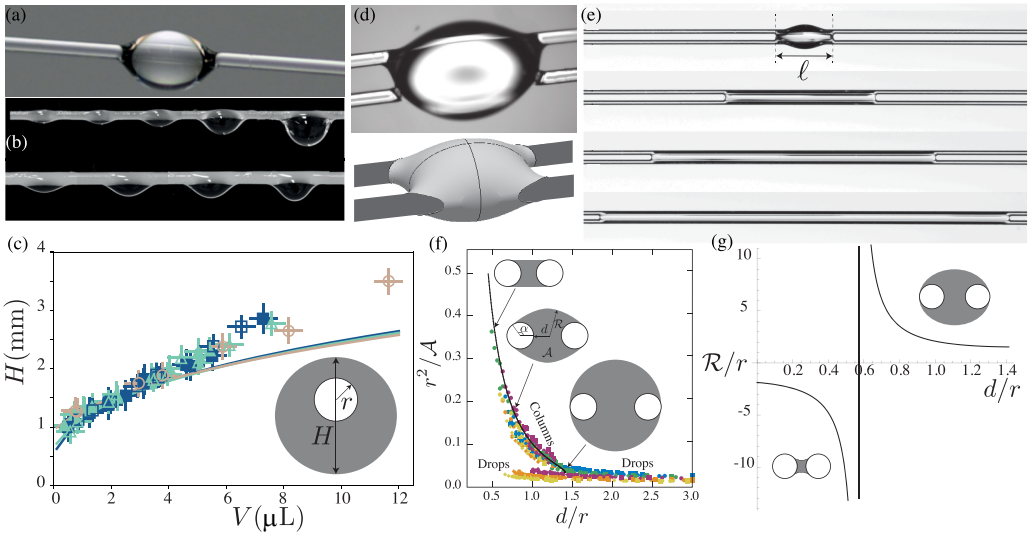

FIG. 2. Perfectly wetting drops on fibers. (a) Silicone oil drop on a glass fiber. (b) Drops of increasing volume V (0.5 to 4 μL) of high-viscosity silicone oil on fibers of radius $r = 0.25$ mm (top) and 0.315 mm (bottom). In that case, there is no swelling during the time of the experiment, and $\ell_c = 1.5$ mm. (c) Height H of a drop of volume V on single fibers of radii $r = 0.233$ mm (open blue squares), 0.350 mm (filled blue squares), 0.293 mm (open green triangles), 0.439 mm (open green triangles), 0.442 mm (open brown circles), and $r = 0.663$ mm (filled brown circles). Lines: predictions from [8]. (d) Drop shape between two fibers, obtained on two glass fibers of radius $r = 0.145$ mm (top) and with surface evolver (bottom). (e) Liquid morphologies adopted by a small volume of liquid on two parallel nylon fibers ($r = 0.2$ mm) for decreasing interfiber distances, from a drop to columns of different lengths ℓ. (f) Normalized liquid length ℓ/V, or equivalently, inverse of the cross-sectional area of liquid $\mathcal{A} = V/\ell$ normalized by r^2, as a function of the dimensionless interfiber distance d/r. The data for several volumes and fiber radii fall onto two branches: drops of small, roughly constant lengths and long columns of constant cross section whose length increases strongly as the interfiber distance is reduced. Line: Prediction of the model of Princen [9]. Inset: Sketches of the cross-sectional shapes of columns where the radius of curvature $\mathcal{R}$ is given by Princen's theory [9], as shown in (g).

which sets its curvature $\kappa(z)$. This balance also defines a typical size, the capillary length $\ell_{cg} = \sqrt{\gamma/(\rho g)}$. We can then define a dimensionless number, the Bond number, that compares the typical size of the drop ℓ to the capillary length such that $\mathrm{Bo} = (\ell/\ell_{cg})^2 = \rho g \ell^2/\gamma$. At small size, $\mathrm{Bo} \ll 1$, and the effect of gravity can be neglected, i.e., the pressure balance leads to a constant curvature $\kappa = c$. The resulting shape, shown in Fig. 2(a), was first described by J. Plateau [7] as an *unduloid* and then formalized by B. J. Carroll [8], who obtained theoretical expressions for the drop length, volume, and height. Here, we consider drops of typical volume $V = 3$ μL on horizontal fibers of typical radii $r = 250$ μm. The drop quickly loses top-bottom symmetry due to gravitational effects as $\mathrm{Bo} \lesssim 1$ [Fig. 2(b)]. As the volume of the drop increases, both its height H and length ℓ increases. The drop's height H follows Carrol's prediction, even as it starts to lose symmetry, until deviating for larger volumes where $H \geqslant \ell_c$; the drop then stretches in the vertical direction below the fiber while keeping a constant length [Fig. 2(c)].

A drop will keep a finite unduloidlike shape when sitting on two separate fibers, although the shape is more complex as the drops adopts a saddle shape between the fibers, with two sleeves extending on each fiber [Fig. 3(d)] [10]. Spreading may, however, occur between the fibers, provided the distance between them is smaller than a critical distance, as was observed early in textile research [Fig. 3(e)] [9,11]. The liquid then adopts the shape of a long liquid column of constant cross section

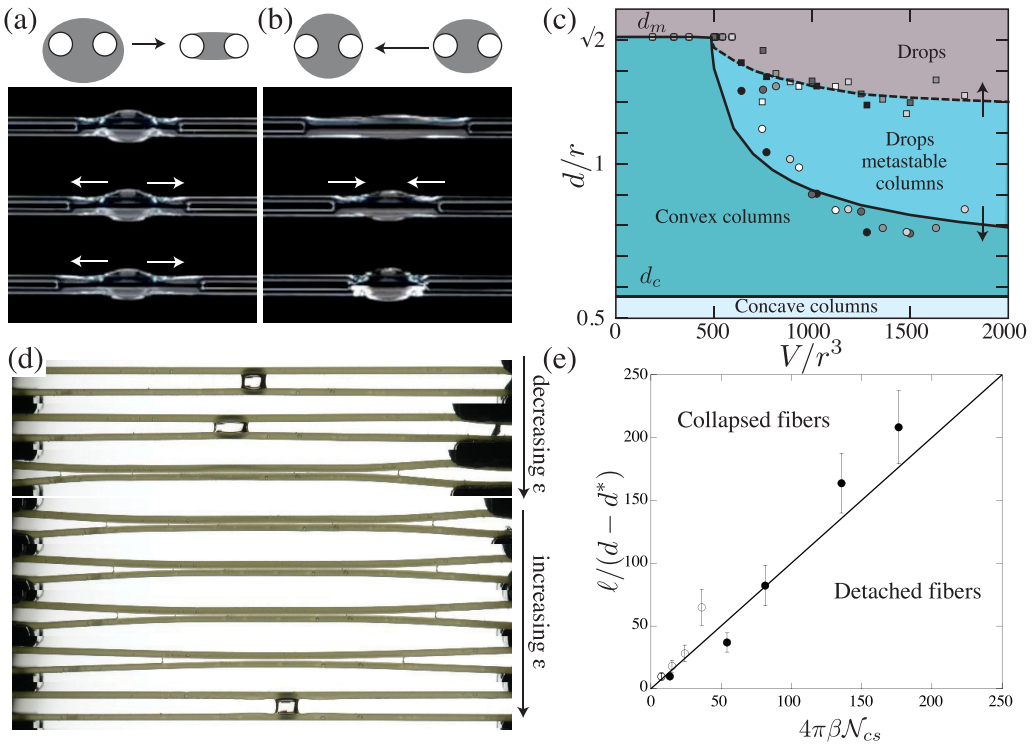

FIG. 3. Spreading transition on parallel fibers. (a) Sketch and chronophotography of the onset of the drop-to-column transition ($r = 150$ μm, $V = 3$ μL, one picture every 2.4 s). (b) Sketch and chronophotography of the column-to-drop transition ($r = 150$ μm, $V = 3$ μL, one picture every 0.16 s). (c) Regime maps showing the existence regions and transitions between drops and columns in the parameter space of the interfiber distance d/r and the drop volume V/r^3. Circles (resp. squares): Experimental drop-to-column and column-to-drop transitions. plain line: Drop to column transition given by $R_d = \mathcal{R}(d)$. Dashed line is a guide for the eyes. (d) Transition between drops and zipped columns on two elastomeric fibers held at both ends (paraffine oil, $r = 250$ μm, on elastomeric fibers of shear modulus $E = 0.5$ MPa) as the strain ϵ in the fiber is increased (reduced) by pulling (releasing) the fibers. (e) Zipping criterion as given by Eq. (4), i.e., critical liquid length ℓ_{zip}, above which the drop spreads and the fibers deform as a function of the elastocapillary stretching number $\mathcal{N}_{cs}$.

$\mathcal{A}$ [Fig. 2(f)], which is characterized by two quantities: the angle α that characterizes the spreading of the drop around the fibers and its radial curvature $\mathcal{R}$ [9,12]. This shape, for which an analytical description can be obtained with a force balance, only depends on the distance between the fibers d/r and evolves from a round column, where $\alpha = \pi$ and $\mathcal{R} = (2d + 2r)$ for $d_m/r = \sqrt{2}$, to a flat column $\alpha = \pi/2$, $\mathcal{R} \to \infty$, for $d_c/r = \pi/2 - 1$, before inverting curvature and being confined between the fibers for smaller interfiber distances [Fig. 2(g)]. Spontaneous imbibition from a bath can only occur if there is a pressure difference between the column and a reservoir at atmospheric pressure, i.e., if the curvature of the column is negative (or $\mathcal{R}$ is negative), that is, for $d/r < \pi/2 - 1$ [13]. However, experiments show that a drop spontaneously spreads as a column for higher interfiber distances, typically, $d/r \simeq 1$. Furthermore, there is a strong hysteresis, i.e., the column coils back to a drop for larger interfiber distances, and there is thus a range of d/r values for which both states coexist [12].

One way to understand this transition is to compute and compare the surface energy of the hemispherical drop and column states as a function of the interfiber distance and drop volume.

This allowed us to obtain a criterion that defines the region of coexisting states, i.e., the region in the parameter space $(d/r, V)$, where columns are only mestastable states, as their surface energy is higher than that of a drop of the same volume [12]. Another approach consists of looking at the spreading dynamics [Fig. 3(a)]. Indeed, the drop adopts a shape with a hemispherical body, flattened by gravity as for the drops on one fiber, and with extending *arms* between the fibers. Spreading may occur as soon as there is a pressure gradient between the arms of the drops and its hemispherical body, which would then drive fluid away from the center of the drop. Between the fibers, the pressure is set by the radius $\mathcal{R}(d)$. Previous surface energy calculation, based on geometry arguments, found that the radius R_d of the hemispherical drop, that lay below the fibers due to gravity, is close to $R_d = 0.7R_{\text{eq}}$, where R_{eq} is the equivalent radius of a spherical drop of the same volume, i.e. $R_{\text{eq}} = (3V/(4\pi))^{(1/3)}$ [12]. We can thus describe the position of spontaneous spreading as $R_d = \mathcal{R}(d)$, in good agreement with the experiments [Fig. 3(c)]. As the volume increases, the transition occurs for smaller interfiber distances. The transition always occurs for $d/r > d_c/r$, i.e., for round convex columns which are unstable to small perturbations. Indeed, if we consider a slight increase of height at one point of the column, there would be a gradient that drives fluid towards the perturbation. This mechanism leads to the column-to-drop transition [Fig. 3(b)]. The radius of curvature of the column reaches a value close to its minimum circular shape $\mathcal{R} = (2d + 2r)$ from $d/r \simeq 1.2$ [Fig. 2(g)]. Indeed, we found that the column-to-drop transition occurs for values $1.2 < d/r < \sqrt{2}$.

Both drops and columns are associated with capillary forces that tend to pull the fibers towards one another. In columns, this force arises from the force acting at the contact line, that increases as α decreases, and the pressure force, that is only positive for concave columns, i.e., for $d/r < \pi/2 - 1$. Both these contributions strongly increase when d/r decreases. For drops, the origin of the capillary force is less obvious due to the complex shape of the drop. However, we can see that a positive pulling force can arise from the asymmetry of the sleeves of the drop along the fibers. As the drop volume increases, the asymmetry of these sleeves decreases, actually resulting in a smaller force. Overall, the force acting on the fibers is always proportional to the wetted length ℓ and can be written

$$F = A\gamma\ell, \tag{2}$$

with a prefactor A that depends on the drop volume [1,14,15]. If the fibers are sufficiently flexible, they may be deformed by this force. These *elastocapillary* effects play a role in various aspects of wetting of fibrous materials [16], for example, in establishing contacts between cellulose fibers in papermaking, drying of fabrics, imbibition of soft fibrous arrays, paintbrushes.... We will consider here the prototypical situation of two horizontal flexible fibers, clamped at both ends, on which we place a single drop [Fig. 3(d)]. The fibers are held under tension (with a prestrain ϵ) at a constant length L. Most of the deformation's energetic cost comes from stretching, and we can neglect bending. Comparing the typical capillary force ($\sim \gamma r$) and tension ($T = E\epsilon\pi r^2$) defines a generic capillary stretching number:

$$\mathcal{N}_{cs} = \frac{E\epsilon r}{\gamma}. \tag{3}$$

If the drop imposes a force sufficient to bring the fibers within the distance at which liquid starts wicking between the fibers, the liquid spreads, the applied force further increases, finally leading to a liquid column between two collapsed fibers. We call this a *zipping* transition [17]. Zipping can be observed either by decreasing the distance between fibers or reducing the prestrain and thus increasing the flexibility of the fibers as shown in Fig. 3(d). The transition can also be triggered by an increase in the capillary force, for example, through a change in drop volume; typically, as the force increases with decreasing volume, spontaneous collapse can happen during drying [1,18]. The condition for zipping to occur, i.e., spontaneous spreading of the drop, can be obtained by writing that the force applied by the drop $F = A\gamma\ell$ overcomes the tension $T = E\epsilon\pi r^2$ to deform the fibers with an angle ϕ such that the distance between the fibers reaches $d^* = Cr$ (with $\pi/2 - 1 < C \leqslant$

1.1), i.e., overcomes a tension $T \sin\phi \simeq T(d - d^*)/L$, which finally writes

$$\frac{\ell}{(d - d^*)} \propto \beta \mathcal{N}_{cs}, \tag{4}$$

where $\beta = r/L$ is the fiber aspect ratio, in good agreement with experiments [Fig. 3(e)]. The transition from the collapsed column back to the drop can also be achieved by increasing the distance between the fibers or increasing the strain within the fibers [Fig. 3(e)], albeit with a strong hysteresis, as the adhesion force is large and the fibers can sustain large deformation before separating or *unzipping* [15].

The formation of liquid columns on pairs of closely space fibers (called *dual fibers*, or *cofibers*) has interesting consequences in various fields. Indeed, for liquid deposited on two fibers, drop growth is prevented below the critical distance d^* as the liquid rather spreads between the fibers. This effect leads to the stabilization of Rayleigh-Plateau instability on cofibers [19] and a higher aerosol collection efficiency for a fog net composed of cofibers [20,21] or flexible fibers that collapse onto one another to spontaneously form cofibers [22].

While this two-fiber system may help in understanding the spreading in a single pore of a fibrous material, in a textile the fibers are generally intertwined, either in a woven (e.g., fabric) or unwoven (e.g., paper) pattern. As a minimalist system, we propose to study the spreading of drops on thin meshes. We consider thin meshes made of nylon fibers woven in a square arrangement with a pore size r_p.

As the liquid spreads, it conforms to the underlying grid and forms a square drop [Fig. 4(a)]. While the liquid does reach a zero contact angle on each fiber [Fig. 4(b)], spreading is stopped by the geometry of the grid to form finite size square-based drops that sit on both sides of the grid [Fig. 4(c)]. Indeed, the liquid is able to penetrate through the thin grid, with a cross-sectional area that is a spherical cap with an apparent contact angle θ_{app} that depends on the mesh's porosity $\phi = r_p^2/(r_p + r)^2$ [Fig. 4(d)]. The drop goes from total spreading ($\theta_{\text{app}} \to 0$) on a low-porosity grid, as it will on a solid surface, to a quasispherical shape ($\theta_{\text{app}} \to \pi$) on a high-porosity grid, as it will on a single fiber. We find that indeed the apparent contact angle increases linearly with ϕ as $\theta_{\text{app}} = 180\phi$.

We have seen here that while spreading is minimal on a fiber even in total wetting conditions (where the liquid readily spreads on flat surfaces), a large spreading can be induced between parallel fibers, provided the interfiber distance is small enough. This spreading is further favored by elasticity, as the deformation of the fibers under the capillary forces applied by the drop spontaneously reduces the distance between the fibers at the drop location. On a network of fibers, the amount of spreading depends on the porosity of the mesh. By changing the pattern of the grid, we can use this system to probe the effect of the anisotropy of the material (i.e., of the fiber orientation). On a material that can absorb the liquid and swell, these different liquid distributions will affect both the absorption dynamics and the final swollen shape, which may interact dynamically with the spreading dynamics.

III. ELASTOMERS AS A MODEL SYSTEM

We choose a model system of a silicone elastomer gel (typically polydimethyl siloxane, PDMS, or polyvynil siloxane, VPS), which is both perfectly wetted and swollen by silicone oils of different viscosities η, that can easily be molded into different shapes, and for which the crosslinking density or chain length (i.e., the Young modulus E and the permeability k) can be easily varied. By changing these material properties as well as the viscosity of the wetting oil, we can probe the effects of different dynamics of spreading, absorption, and deformation. In particular, the absorption and deformation of the material are characterized by two quantities: the maximum swelling ratio, i.e., the maximum change of volume upon swelling λ_{max} or the maximum concentration of solvent c_{max} in the material, and the poroelastic effective diffusion coefficient $\mathcal{D}^*$ that characterizes the swelling dynamics.

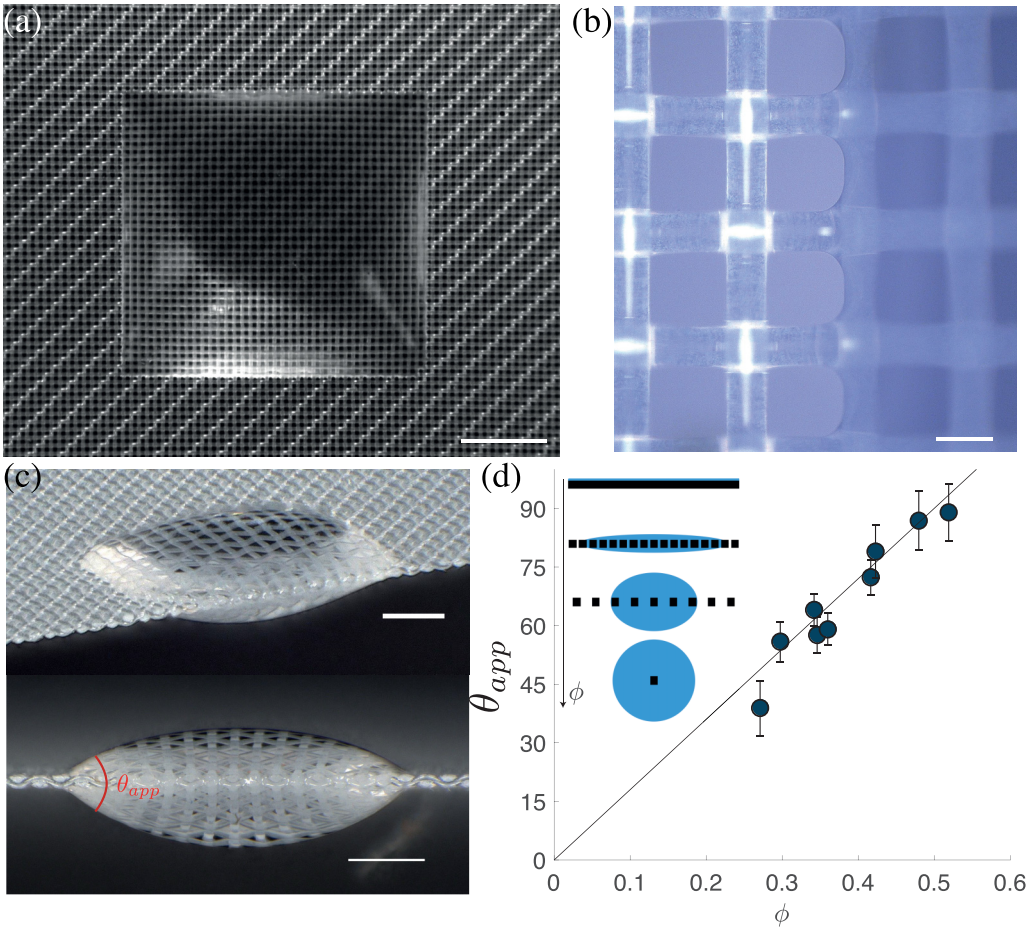

FIG. 4. Spreading on woven meshes. (a) Image of a silicone oil square drop on a thin woven nylon square mesh from the top ($r = 35$ µm, $r_p = 42$ µm, $\phi = 0.3$), scale bar 1 mm. (b) Zoom on the drop's edge, scale bar 100 µm. (c) View from the side ($r = 50$ µm, $r_p = 91$ µm, $\phi = 0.42$), exhibiting an apparent contact angle θ_{app}. Scale bar 500 µm. (d) Evolution of θ_{app} with ϕ. Line given by $\theta_{\text{app}} = 180\phi$. Sketch in inset: On nonporous surfaces ($\phi = 0$), the liquid will spread until reaching a layer of molecular thickness ($\theta_{\text{app}} \simeq 0$), while on a single fiber ($\phi = 1$) it will adopt a quasispherical shape ($\theta_{\text{app}} \simeq \pi$) with intermediate shapes for intermediate porosities.

The poroelastic gel, with an initial prestrain ϵ, solvent concentration c_0, and chemical potential μ_0, is placed in contact with a reservoir of solvent (typically a drop) at chemical potential $\mu \neq \mu_0$, which causes swelling, i.e., a diffusion of the solvent in the material coupled with a deformation characterized by a displacement field $\mathbf{u}$. We consider that both the solvent and the polymer are incompressible, and that we are at mechanical equilibrium. The concentration of solvent follows [23,24],

$$\frac{\partial c}{\partial t} = \mathcal{D}^* \nabla^2 c, \tag{5}$$

with the effective poroelastic diffusion coefficient

$$\mathcal{D}^* = \frac{Gk}{\eta} \frac{2(1-\nu)}{1-2\nu}, \tag{6}$$

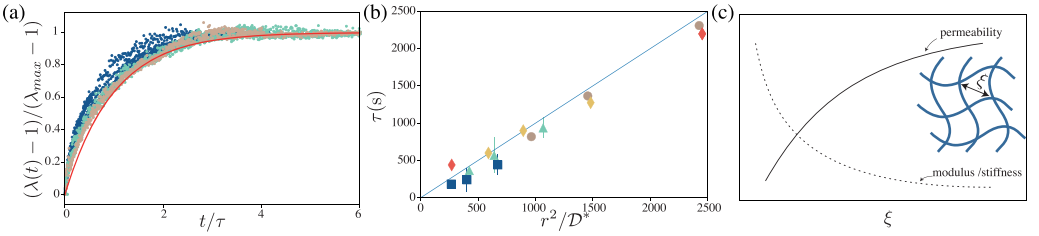

FIG. 5. Swelling dynamics of an elastomeric fiber immersed in silicone oil. (a) Evolution of the swelling ratio $\lambda(t) = r(t)/r(0) = \ell(t)/\ell(0)$, normalized by the maximal swelling ratio $\lambda_{\max}$, as a function of the time normalized by the characteristic swelling time τ for fibers immersed in silicone oil [$\eta = 2.3$ mPa s (dark blue), $\eta = 3$ mPa s (light blue), and $\eta = 5.4$ mPa s (brown)] and various fiber radii [$r(0) = 250$, 315, and 475 μm]. (b) Swelling time τ as a function of fiber radius and diffusion coefficient for VPS 32 [$r(0) = 250$ (blue squares), 315 (light blue triangles), and 475 μm) (brown circles)], VPS 8 [$r(0) = 475$ μm, red diamonds], and PDMS [$r(0) = 442$ μm, yellow diamonds]. (c) Sketch showing the evolution of modulus G and permeability k with typical mesh size ξ.

where ν is the poroelastic Poisson's ratio, which characterizes the ability of the material to swell [23] (we take $\nu = 0.3$ which is typical for the gels we are considering [23]), and G is the shear modulus, which is related to the Young modulus $E = 2G(1 + \nu_e)$ with the elastic Poisson's ratio ν_e (equal to 1/2 for an incompressible gel, as we will consider here). We only consider linear poroelasticity, i.e., $\mathcal{D}^*$, E, and k are considered constants. The maximum solvent concentration $c_{\max}$ depends on the material through $\mathcal{D}^*$, the molecular volume Ω, and the residual strain ϵ; the swelling ratio indeed increases with increasing strain, i.e., a material under tension can absorb more solvent.

We probe this poroelastic dynamics with our system by molding the elastomer into a fiber and immersing it in a bath of oil. We measure the evolution of the length L and radius r of the fiber (Fig. 5). Both evolve with the same dynamics, i.e., the swelling is isotropic, and the swelling ratio is defined as $\lambda(t) \equiv L(t)/L_0 \simeq r(t)/r_0$. At first order, the swelling dynamics is exponential until reaching a plateau at $\lambda_{\max}$ and time τ [Fig. 5(a)] [25]. The typical timescale of this poroelastic diffusion is then given by

$$\tau = \frac{r^2}{\mathcal{D}^*}, \tag{7}$$

as shown in Fig. 5(b). We verify that $\mathcal{D}^*$ is inversely proportional to the viscosity. For a given viscosity $\eta = 2.3$ mPa s, we obtain $\mathcal{D}^* = 2.31 \times 10^{-10}\,\mathrm{m^2\,s^{-1}}$ for VPS 8 [26]. Elite double 8 Zhermarck ($E = 0.2$ MPa), $2.34 \times 10^{-10}\,\mathrm{m^2\,s^{-1}}$ for VPS 32 [27] ($E = 0.9$ MPa) and $1.68 \times 10^{-10}\,\mathrm{m^2\,s^{-1}}$ for PDMS [28] ($E \simeq 1.5$ MPa). Interestingly, the value of $\mathcal{D}^*$ is almost constant for all materials used. Indeed, the effective diffusion coefficient depends on the ratio Ek/η; when increasing the length of the polymer chain, or the distance between crosslinks ξ, there is both a decrease in the Young modulus (the material is softer) and an increase in permeability (the material is more permeable), resulting in small variations of the product Ek [Fig. 5(c)]. The maximal swelling ratio remains close to $\lambda = 1.5 \pm 0.05$ in all our experiments.

This system allows us to vary the swelling timescale τ by varying the geometry (e.g., the radius r for fibers) and the oil viscosity η, with typical times of a few to tens of minutes.

IV. COMBINED WETTING, ABSORPTION, AND SWELLING OF A DROP ON A FLAT SURFACE

We start by placing a single drop on the flat surface of an elastomer block. The drop spreads rapidly and slows down as it is simultaneously absorbed in the substrate. The spreading is eventually stopped, and the drop reaches a maximal radius $R_{\max}$ before retracting and being fully absorbed in

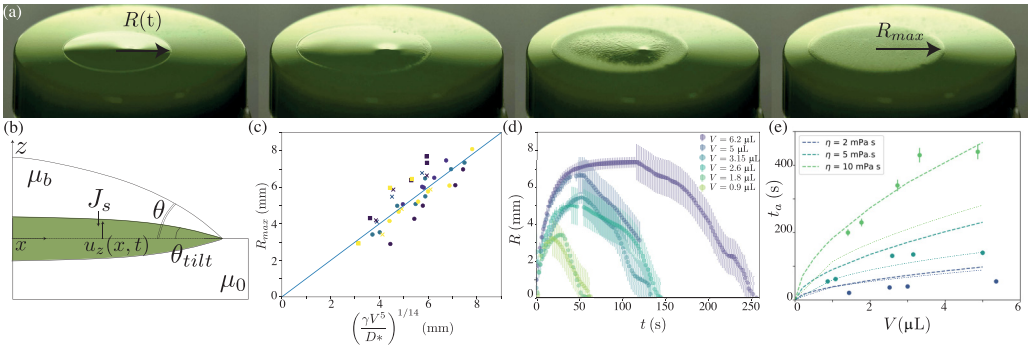

FIG. 6. Swelling dynamics of a drop on a flat elastomer. (a) Chronophotographies of the spreading of a drop of silicone oil ($\eta = 2.3$ mPa s), $V = 4$ µL on a VPS 32 substrate (one picture every 10 s). (b) Sketch of the swelling of the underlying substrate. (c) Maximal drop radius $R_{\max}$ as a function of the scaling Eq. (11) for different substrates (crosses VPS8, circles VPS 32, squares PDMS) and oil viscosities ($\eta = 2.3$ mPa s yellow, 5.4 mPa s blue, and 10.5 mPa s purple). (d) Evolution of the radius of the drop measured for different initial drop volumes ($\eta = 5.3$ mPa s on VPS 32). (e) Total absorption times as a function of drop volume obtained experimentally (circles) and with a model taking into account the substrate deformation θ_{tilt} (dashed lines), or not taking into account this deformation (dotted lines).

the material, leaving a swollen imprint of radius $R_{\max}$ after a typical absorption time of a few minutes [Fig. 6(a)] [29].

A sketch of the problem is shown in Fig. 6(b). As soon as the drop is in contact with the elastomer, the liquid diffuses vertically into the substrate with a flux J_s, resulting in a vertical deformation $u_z(x,t)$. We assume that the system remains axisymmetric and that the liquid only diffuses vertically, i.e., we neglect radial diffusion within the elastomer as the drops are much wider than thick. The drop spreads with an apparent contact angle $\theta(t)$; as the wetting front advances, more solid is in contact with a liquid, leading to more absorption and deformation of the substrate, until eventually the liquid starts receding as more volume is absorbed below the drop. The maximum radius is thus reached at the moment the absorption balances the surface tension-driven spreading. We assume that the drop adopts the shape of a spherical cap at all times, with an apparent contact angle θ such that

$$R^3 = 4V/(\pi\theta). \tag{8}$$

We can then model the spreading dynamics using Tanner's law, i.e., assuming the driving capillary forces are mostly dissipated with viscous flows in the corners at the edges of the drop; hence the apparent contact angle evolves as $\theta^3 \sim (\eta/\gamma)\mathrm{d}R/\mathrm{d}t$. This yields the evolution of the spreading radius $R^{10}(t) \sim \gamma V^3 t/\eta$, from which we can extract a typical spreading time

$$t_{\text{spread}} \sim \frac{R_{\max}^{10}\eta}{\gamma V^3}. \tag{9}$$

To construct an absorption timescale, we consider that the liquid diffuses vertically over a typical distance $L = V/(\pi R_{\max}^2)$, i.e.,

$$t_{\text{swell}} = \frac{L^2}{\mathcal{D}^*} \sim \frac{V^2}{R_{\max}^4 \mathcal{D}^*}. \tag{10}$$

As seen above, $\mathcal{D}^* \propto Ek/\eta$. The maximum radius, given by $t_{\text{spread}} = t_{\text{swell}}$, thus becomes

$$R_{\max} \sim \left(\frac{\gamma V^5}{Ek}\right)^{1/14}, \tag{11}$$

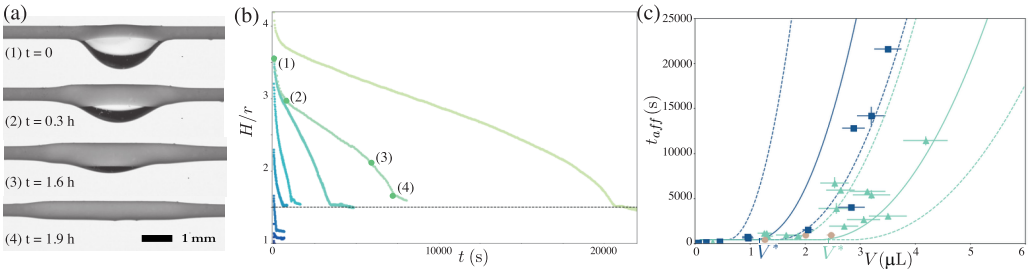

FIG. 7. Swelling dynamics of a drop on an elastomer fiber. (a) Chronophotography of a silicone oil droplet ($\eta = 2.3$ mPa s, $V = 2$ μL) absorbed on a VPS 32 fiber ($r = 223$ μm). (b) Evolution of the drop's height H as a function of time for different initial volumes ($V = 0.05, 0.1, 0.5, 1.4, 3.2, 4.1, 3.9, 5.7$ μL). (c) Total absorption time t_a as a function of drop volume for $r = 233$ μm (blue), $r = 293$ μm (green), and $r = 442$ μm (brown). The full lines represent the predicted absorption time, with the average measured radius and swelling ratio in the stretched state given by Eq. (13), while the dashed lines represent the variability due to the uncertainty in measuring the fiber radius and the swelling ratio.

which is remarkably independent of viscosity, as both spreading and poroelastic diffusion timescales are proportional to viscosity. While the exponent is difficult to evaluate in the experiments since the radii only span below 1 cm, all our data for various elastomer or viscous oils do collapse onto a single curve, in good agreement with this scaling [Fig. 6(c)]. To describe the complete dynamics [Fig. 6(d)], we need to couple the spreading law, which gives an advancing speed, to the change in volume $V(t)$ given by the integration of the diffusive flux J_s, which generates a receding speed. Furthermore, as the substrate absorbs liquid and deforms, the angle of the drop decreases in the vicinity of the contact line with an angle $\theta_{\text{tilt}} = -\partial u_z/\partial x$ such that

$$\theta = \frac{4V}{\pi R^3} + \frac{\partial u_z}{\partial x}(R, 0, t), \tag{12}$$

which slows down the spreading, as seen in the plateau in $R(t)$ before receding [Fig. 6(d)]. We note that this is different from the simultaneous spreading and absorption of a drop on a nondeformable porous substrate, where there is no such change of slope, and the radius adopts a sharp bell-shape curve [30]. This deformation-induced slowdown affects the total absorption time t_a, as it reduces how fast the solvent can reach "dry" unswollen region [Fig. 6(e)]. Indeed, the total absorption time is a combination of the speed of the diffusive absorption, which occurs over a time τ, and spreading, which allows more material to be in contact with the liquid, i.e., the surface over which liquid can be absorbed. This is true because the diffusion directly from the liquid to a region with no solvent is much faster than the diffusion of the solvent from the swollen region to dry regions deeper into the material. Indeed, while the absorption time is of the order of a few minutes here, it will take hours for the solvent to redistribute into the block of elastomer and finally flatten the swollen imprint on the surface. This illustrates the importance of the liquid distribution on the absorption dynamics, an effect that will be crucial for fibrous systems where the geometry can hinder or favor spreading.

V. DROPS ON SWELLING FIBERS

A. Absorption dynamics

Indeed, on a fiber spreading is minimal, and the liquid adopts a compact barrel (or unduloid) shape. The portion of the fiber directly below the drop swells and is quickly saturated with liquid [Fig. 7(a)], with a dynamic similar to that of an immersed fiber, as shown by the initial exponential decrease of the drop height H over a timescale τ [Fig. 7(b)] [31]. A portion of the drop volume V^* is thus absorbed, leaving a drop of remaining volume $(V - V^*)$ sitting on a saturated swollen fiber. The solvent then diffuses away into the unsaturated parts of the fiber with a slower dynamics. In order to

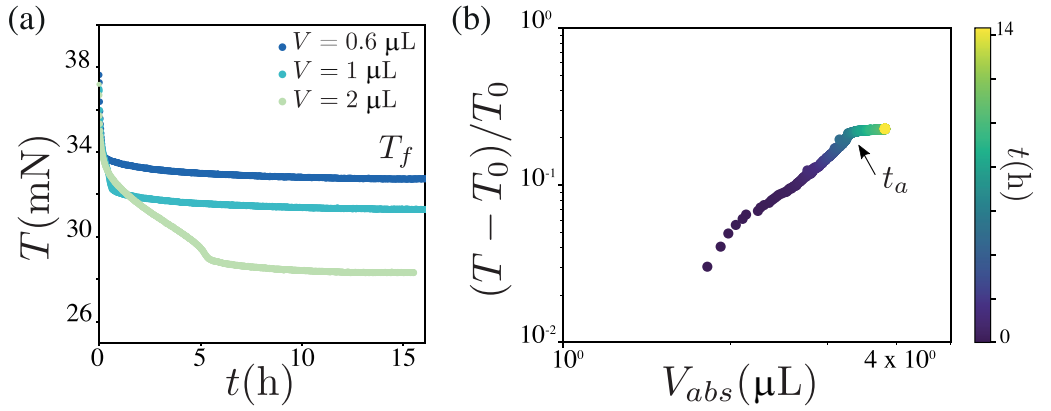

FIG. 8. Swelling and tension. (a) Measured tension in a fiber of radius $r = 250$ µm during the absorption of a single drop of silicone oil ($\eta = 5.4$ mPa s) of various initial volumes. (b) Evolution of the tension as a function of absorbed volume.

absorb the remaining volume, the liquid has to travel over a length $\ell_d = [(V - V^*)/2]/[\pi r^2(\lambda^2 - 1)]$ on both sides of the drop (taking into account the fact that the fiber swells up to a radius λr) with a typical timescale $\ell_d^2/\mathcal{D}^*$, yielding a total absorption time:

$$t_a = \tau + \frac{(V - V^*)^2}{4\pi^2 \mathcal{D}^* r^4 (\lambda^2 - 1)^2}. \tag{13}$$

The absorption time thus strongly increases with the drop volume [Fig. 7(c)]. Below the critical volume V^*, the drop is fully absorbed by the initial exponential swelling with a timescale τ. A slight increase in volume then leads to a strong increase of absorption time due to the slow diffusion required to absorb the remaining volume, with typical absorption times orders of magnitude higher. As a comparison, a microliter silicone oil drop absorbed within minutes on a flat VPS elastomer, where it can spread, will typically take 10 hours to be absorbed on a thin fiber of the same material where it remains compact [Figs. 6(e) and 7(c)]. In general, one can decrease the absorption time by favoring motion of the drop towards nonswollen regions, or inducing spreading. The absorption time of the same drop between two fibers, where the drop spreads over long distances as a liquid column, is indeed reduced to a few seconds. As seen earlier, it is important to take into account elastocapillary effects to predict this spreading transition. For that, we need to know the tension within the fiber in particular, as it may vary during swelling, as we shall discuss in the next section.

B. Fiber tension

As the fiber absorbs fluid, it swells in all directions, i.e., both the radius and length must increase by a factor λ. In our experiments, fibers are held at a constant length L, as will be the case in a network where the distance between nodes is fixed. This implies that the tension in the fiber must decrease to accommodate for the swelling. We measure the tension T in the fiber as a drop is absorbed [Fig. 8(a)] using a force sensor attached to one end of the fiber. Indeed, the tension decreases from its initial value $T_0 = \pi r^2 E \epsilon_0$ with a dynamics that follows exactly the absorption dynamics [i.e., the evolution of $H(t)$ given in Fig. 7(b)]. The final drop in tension increases with the volume of the drop. From the shape of the drop, we can deduce its volume [as shown in Fig. 2(c)] at all times, i.e., estimate the absorbed volume $V_{\text{abs}}(t)$. There is a direct relation between the absorbed volume and the change in tension that seems to follow a scaling law $\Delta T \propto V_{\text{abs}}^3$, although we do not have arguments to explain this observation [Fig. 8(b)]. We note here that the change of tension is global, while the swelling remains localized at the position of the drop. Indeed, there is a swollen

FIG. 9. Swelling-induced zipping. (a) Chronophotography of the absorption of a silicone oil drop ($\eta = 2$ mPa s) between two VPS 32 fibers of radius $r = 250$ μm (one picture every 200 ms). (b) Measured evolution of the deformation $\ell/(d - d^*)$ as a function of the fiber tension through the capillary stretching number $\mathcal{N}_{cs}$. Here the tension is measured with a force sensor, and the other quantities are measured on photographs. Line given by Eq. (4).

region [Fig. 7(a)], which remains for long times as the solvent slowly diffuses away into the rest of the fiber over timescales which become comparable to evaporation (typically days); the fiber generally returns to its original state before the solvent can reach a homogeneous concentration.

This change of tension has important consequences. We have seen earlier that the swelling ratio increases with increasing strain, and thus the maximum concentration of solvent that is possible to have in the fiber will decrease as strain decreases during absorption. One consequence of this is a transient *deswelling* of saturated regions that is observed when several drops are placed on a single fiber. Indeed, fluid is seen to escape the saturated region of the fiber to form drops on its surface as the tension decreases due to the absorption of liquid from nearby drops [32]. The emergence of liquid on the fiber surface may then induce coalescences between neighboring drops, which further reduces spreading of the liquid and significantly increases absorption time (up to tens of hours). This deswelling and drop motions are a direct consequence of a local saturation, due to the compact shape of drops on fibers, and a global decrease of tension due to the absorption of other drops (even far away) on the same fiber, which highlights again the importance of the liquid distribution on such swelling-spreading coupled dynamics. Furthermore, the fiber becomes more deformable as fluid is absorbed and tension (or strain ϵ) decreases, as the effective modulus $E\epsilon$ decreases, which will favor elastocapillary deformations, as we will see in the next section.

C. Zipping

We now consider two parallel fibers attached at both ends under a strain ϵ. As seen before, below a critical distance, a drop will spontaneously spread as a liquid column. In the case of swelling fibers, the solvent is quickly absorbed by the fibers from this column (in typically hundreds of seconds), and the change of length and tension may lead to deformation (e.g., sagging of the fibers). If the fibers are further apart, the liquid first adopts a compact drop shape, from which it slowly diffuses in the fibers. As the fibers swell, there is a simultaneous increase in fiber diameter and decrease in tension, which both lead to a spreading of the drop, i.e,. an increase of drop length ℓ and thus of the exerted capillary force $\gamma\ell$ [Fig. 9(a)]. All of these effects favor the zipping transition, as evidenced by the criterion given in Eq. (4). Indeed, there is both an increase in $\ell(t)/[d(t) - d^*]$ and a decrease in $\mathcal{N}_{cs}(t)$. The swelling can thus induce zipping [Fig. 9(a)], as shown by the measurements in Fig. 9(b). During absorption, the decrease in $\mathcal{N}_{cs}(t)$ and increase in $\ell(t)/[d(t) - d^*]$ concur to cross the line given by Eq. (4), leading to zipping and a fast absorption (and thus a rapid decrease in drop length) as shown with the blue curve. The transition is therefore dependent on the initial tension and distance between the fibers, as well as drop volume; indeed, there needs to be enough reservoir in the drop in order to induce sufficient swelling to cross the line before all the drop is absorbed [see red curves in Fig. 9(b) for cases where no zipping was observed].

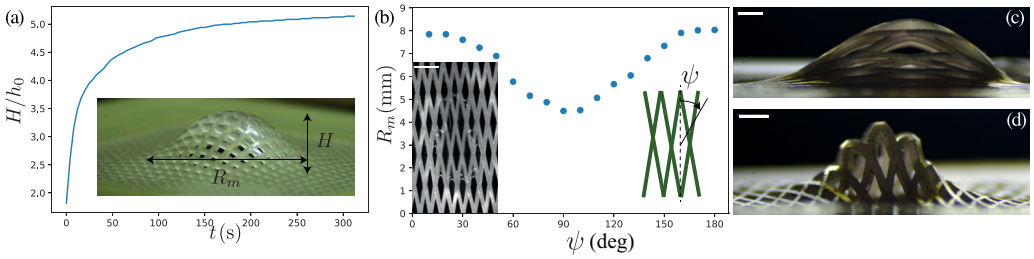

FIG. 10. Swelling thin grids. (a) Evolution of the deformation H of a thin VPS 32 square grid, normalized by the initial thickness of the grid elements h_0, during the absorption of a silicone oil drop ($\eta = 2$ mPa s). Inset: Final shape with a height H of 1 mm. (b) Evolution of the extension radius R_m as a function of angle ψ on an anisotropic VPS 16 grid after the absorption of a silicone oil drop ($\eta = 2$ mPa s). Insets: Initial shape of the drop deposited on the pattern (scale bar 2 mm) and definition of the geometry. Image of the final shape in (c) the direction of the main axis ($\psi = 0°$) and (d) in the perpendicular direction ($\psi = 90°$). Scale bars: 1 mm.

We note that the final absorption time is strongly reduced compared to the case of a single fiber; indeed, here absorption occurs within tens of seconds, as zipping induces a fast spreading, leading to liquid in contact with a large portion of unsaturated fiber. This absorption time is given by the swelling timescale τ and the spreading-zipping dynamics, which depends both on poroelastic and elastocapillary effects. We have recently investigated this combined dynamics by looking at the spontaneous capillary imbibition between two fibers from a bath and show that swelling may accelerate imbibition, as it decreases the distance between the fibers at the meniscus' position and thus increases the capillary driving force [33]. Here again, the decrease in interfiber distance is due to a combination and reinforcement of several mechanisms: swelling and increase of fiber radius, a decrease in tension that both induces a change in fiber diameter with the relaxation of the axial constraint (the elastomer has an elastic Poisson's ratio of 1/2) and favors the elastic deformation induced by the capillary forces at the meniscus, until eventually leading to zipping and collapse of the fibers.

D. Swelling grids

Finally, as a last step towards more complex woven or nonwoven textiles, we investigate the spreading of drops on model poroelastic grids made of VPS elastomer. The grids are molded on micromilled engraved brass. This technique allows to accurately control the grid's pattern and the thickness of its elements (typically $h_0 = 250$ μm, with similar pore sizes). Contrary to the woven meshes, the surface is flat and the *fibers* (or grid segments) are of square cross section. We start with a square grid, similar to the ones presented in Fig. 4. As a drop is deposited, it spreads on the surface to reach a finite size; simultaneously, it absorbs into the material, leading to a local swelling of the grid. As the mesh is very thin, this local increase of thickness immediately leads to a large out-of-plane deformation [Fig. 10(a)].The deformation H increases quickly, with a timescale close to the swelling timescale τ (typically $\tau = h_0^2/\mathcal{D}^* \simeq 250$ s for an initial thickness $h_0 = 250$ μm). The final bump has a finite radius R_m, that we measure as the extension of the hump's base at a height $0.9H_{\max}$ from the point of maximum height $H_{\max}$ [inset in Fig. 10(a)]. We introduce an anisotropy in the pattern by tuning the angle between elements, from square to rhombus, effectively creating a main direction of the fibers (along the long axis of the rhombus). In that case the deformation is not axisymmetric anymore but forms an elongated hump, as shown by the evolution of the radius R_m along several directions ψ [Fig. 10(b)]. The hump has a maximal extent in the main direction of the fibers [Fig. 10(c)] and a minimal extent in the orthogonal direction [Fig. 10(d)]. This anisotropy is due to two combined effects: first, the spreading of the drop conforms to the grid pattern and is thus more elongated along the main fiber direction [inset, Fig. 10(b)], and second, the deformation is less costly orthogonally to the fibers, as the bending rigidity is higher in the fiber direction compared

to the transverse direction. These considerations are also true for our copy paper sheets (Fig. 1); the bending rigidity is higher in the machine direction, i.e., along the main direction of the fibers, and the spreading and absorption is anisotropic. In that case the swelling-induced wrinkles also exhibit anisotropic bulges that are thinner in the transverse direction and aligned with the main fiber direction.

VI. CONCLUSION

Spreading on fibrous materials is often accompanied by imbibition and swelling of the fibers (e.g., a drop of water on a piece of paper). Swelling is a pseudodiffusive process, with an effective poroelastic diffusion coefficient $\mathcal{D}^*$ that defines a typical absorption timescale $\tau = \ell^2/\mathcal{D}^*$ for materials of size ℓ. However, the total absorption time strongly depends on the spreading dynamics, and thus on the geometry of the substrate that determines the drop shape. Using model systems of increasing complexity, from flat surfaces to fibrous grids, we have shown that while it typically takes a minute to absorb a microliter drop onto an elastomer, this time is multiplied to reach several hours on a fiber of the same material. This time can be strongly reduced, down to tens of seconds, if the liquid is allowed to spread, e.g., in a pore consisting of two fibers or on a grid. This absorption and swelling lead to a decrease in tension and deformation of the material, which may slow down spreading due to a deformation of the contact line on a flat surface but more often favors spreading and thus accelerates absorption (e.g., between fibers). Localized swelling can further lead to large-scale deformations as the one observed on thin grids. In that case, as for water on paper, the final shape strongly depends on the underlying structure, i.e., the arrangements of the fibers. While such deformations may be detrimental in some situations (e.g., in printing or packaging), it could be harnessed to initiate and control large-scale motions passively. Indeed, deformations induced by moisture absorption in layers of materials made of cellulose fibers with different orientations are the origin of the hygroscopic movements of several plants [34]. The model systems presented here may serve as the base mechanisms to better characterize, model, and design such materials.

ACKNOWLEDGMENTS

We thank all of our collaborators that have contributed to this topic over the years, in particular, Julien Dervaux, Howard Stone, and Christophe Josserand, as well as the students that played an important role in preliminary and final experiments, in particular, Nsemi Nsimba, Alexander Mitranescu, Rong Luo, and Nathalie Fabre-Parras. C.D. acknowledges Hugues Lepic and the Fondation de l'École Polytechnique for funding through the Chaire Professorale Jean Marjoulet, and the European Union for funding through a consolidator grant (ERC ElCapiTex-101087747).

[1] C. Duprat, Moisture in textiles, Annu. Rev. Fluid Mech. **54**, 443 (2022).

[2] C.-L. Wong, S. Wang, S. Karimnejad, M. G. Wijburg, H. Mansouri, and A. A. Darhuber, Transient deformation and swelling of paper by aqueous co-solvent solutions, Soft Matter **19**, 1202 (2023).

[3] C. G. van der Sman, E. Bosco, and R. H. J. Peerlings, A model for moisture-induced dimensional instability in printing paper, Nordic Pulp Pap. Res. J. **31**, 676 (2016).

[4] A.-L. Erkkilä, P. Pakarinen, and M. Odell, Sheet forming studies using layered orientation analysis: Can lead to a better understanding of the drainage process, Pulp Paper Canada **99**, 81 (1998).

[5] T. Enomae, Y.-H. Han, and A. Isogai, Nondestructive determination of fiber orientation distribution of paper surface by image analysis, Nordic Pulp Pap. Res. J. **21**, 253 (2006).

[6] G. Kloppenburg, X. Li, A. Dinkelmann, H. Finckh, J. Neumann, and J.-W. Simon, Functional description of fiber orientation in paperboard based on orientation tensors resulting from μ-CT scans, Cellulose **31**, 7865 (2024).

[7] J. Plateau, Recherches expérimentales et théoriques sur les figures d'équilibre d'une masse liquide sans pesanteur (3e série), Mem. Acad. R. Belg. **30**, 1 (1857).
[8] B. J. Carroll, The accurate measurement of contact angle, phase contact areas, drop volume, and laplace excess pressure in drop-on-fiber systems, J. Colloid Interface Sci. **57**, 488 (1976).
[9] H. M. Princen, Capillary phenomena in assemblies of parallel cylinders, III. Liquid columns between horizontal parallel cylinders, J. Colloid Interface Sci. **34**, 171 (1970).
[10] A. Bedarkar, X.-F. Wu, and A. Vaynberg, Wetting of liquid droplets on two parallel filaments, Appl. Surf. Sci. **256**, 7260 (2010).
[11] F. W. Minor, A. M. Schwartz, E. A. Wulkow, and L. C. Buckles, The migration of liquids in textile assemblies, Part III: The behavior of liquids on single textile fibers, Text. Res. J. **29**, 940 (1959).
[12] S. Protiere, C. Duprat, and H. A. Stone, Wetting on two parallel fibers: Drop to column transitions, Soft Matter **9**, 271 (2013).
[13] R. V. Dyba and B. Miller, Evaluation of wettability from capillary rise between filaments, Text. Res. J. **39**, 962 (1969).
[14] C. Duprat, S. Protiere, A. Y. Beebe, and H. A. Stone, Wetting of flexible fibre arrays, Nature (London) **482**, 510 (2012).
[15] C. Duprat, C. Nous, and S. Protiere, Controlling wet adhesion with elasticity, Soft Matter **16**, 6463 (2020).
[16] J. Bico, E. Reyssat, and B. Roman, Elastocapillarity: When surface tension deforms elastic solids, Annu. Rev. Fluid Mech. **50**, 629 (2018).
[17] C. Duprat and S. Protiere, Capillary stretching of fibers, Europhys. Lett. **111**, 56006 (2015).
[18] C. Duprat, A. D. Bick, P. B. Warren, and H. A. Stone, Evaporation of drops on two parallel fibers: Influence of the liquid morphology and fiber elasticity, Langmuir **29**, 7857 (2013).
[19] P. Wang, J. Zhou, B. Xu, C. Lu, Q. Meng, and H. Liu, Bioinspired anti-plateau-Rayleigh-instability on dual parallel fibers, Adv. Mater. **32**, 2003453 (2020).
[20] R. Labbé and C. Duprat, Capturing aerosol droplets with fibers, Soft Matter **15**, 6946 (2019).
[21] A. Moncuquet, A. Mitranescu, O. C. Marchand, S. Ramananarivo, and C. Duprat, Collecting fog with vertical fibres: Combined laboratory and in-situ study, Atmos. Res. **277**, 106312 (2022).
[22] A. Rewakowicz, J.-M. Chomaz, and C. Duprat, Mist collector: Art and science project, in *Proceedings of the 7th International Conference on Fog, Fog Collection and Dew, Wrocław, Poland*, edited by M. Błaś and M. Sobik (Uniwersytet Wrocławski, Wrocław, 2016).
[23] J. Yoon, S. Cai, Z. Suo, and R. C. Hayward, Poroelastic swelling kinetics of thin hydrogel layers: Comparison of theory and experiment, Soft Matter **6**, 6004 (2010).
[24] C. Kopecz-Muller, V. Bertin, E. Raphaël, J. D. McGraw, and T. Salez, Mechanical response of a thick poroelastic gel in contactless colloidal-probe rheology, Proc. R. Soc. A **479**, 20220832 (2023).
[25] More exactly, the radius variation $\Delta r(t) = r(t) - r_0$ in time follows $\frac{\Delta r(t)}{\Delta r(t=\infty)} = 1 - \sum_{n=1}^{\infty} \frac{4^{-\alpha_n^2 t/\tau}}{\alpha_n^2}$, with α_n the nth zero of the Bessel function of order 0.
[26] Elite double 8 Zhermarck.
[27] Elite double 32 Zhermarck.
[28] Sylgard 182, PDMS to curing agent ratio 10:1.
[29] P. Van de Velde, N. Fabre-Parras, C. Josserand, C. Duprat, and S. Protière, Spreading and absorption of a drop on a swelling surface, Europhys. Lett. **144**, 33001 (2023).
[30] V. M. Starov, S. R. Kostvintsev, V. D. Sobolev, M. G. Velarde, and S. A. Zhdanov, Spreading of liquid drops over dry porous layers: Complete wetting case, J. Colloid Interface Sci. **252**, 397 (2002).
[31] P. Van de Velde, S. Protière, and C. Duprat, Dynamics of drop absorption by a swelling fiber, Soft Matter **17**, 6168 (2021).
[32] P. Van de Velde, J. Dervaux, S. Protière, and C. Duprat, Spontaneous localized fluid release on swelling fibres, Soft Matter **18**, 4565 (2022).
[33] P. Van de Velde, J. Dervaux, C. Duprat, and S. Protière, Imbibition and collapse between swelling fibres, J. Fluid Mech. **978**, A2 (2024).
[34] I. Burgert and P. Fratzl, Actuation systems in plants as prototypes for bioinspired devices, Philos. Trans. R. Soc. A **367**, 1541 (2009).